



# Wave-turbulence separation at a tidal energy site with empirical orthogonal function analysis

M. Togneri<sup>\*</sup>, I. Masters, I. Fairley

College of Engineering, Swansea University Bay Campus, SA1 8EN, United Kingdom

## ARTICLE INFO

### Keywords:

Waves  
Turbulence  
Turbulent kinetic energy  
Empirical orthogonal analysis  
Tidal power

## ABSTRACT

Acoustic Doppler current profilers (ADCPs) are the standard tool for measuring tidal currents at tidal stream energy sites; they are used to estimate several parameters, including turbulent kinetic energy (TKE). However, estimates of TKE from ADCPs are often swamped by wave action. We surmise that this bias can be detected as a data mode: to test this, we present an empirical orthogonal function (EOF) analysis of two months of TKE estimates from ADCP measurements at a tidal energy site with significant wave activity. The results of the analysis were compared with linear wave theory, using data from a wave buoy. The first data mode identified from EOF analysis agrees well with the wave bias predicted by linear theory, and the resulting decomposition of the data set into wave and turbulent components appears realistic. This decomposition is possible from ADCP data alone, and therefore offers a novel and widely applicable analysis technique for simultaneous assessment of turbulence and waves at highly-energetic tidal sites. The method can also be applied retrospectively to historical data sets. We also show that the decomposition can be improved by including higher EOF modes, but this requires an independent measurement of waves to determine the optimum number of modes.

## 1. Introduction

The combined action of waves and turbulence in energetic tidal currents is the strongest contributor to load variability on tidal energy converters (TECs) (Milne et al., 2016; Elasha et al., 2017; McCann, 2007). Quantifying these phenomena from field measurements at actual or potential deployment sites, however, is not a trivial task. The most widely-employed tools for measurement of flow conditions are acoustic Doppler current profilers (ADCPs); these are recommended by IEC standards (IEC/TS 62600-201) and therefore effectively required in an industrial context. It is quite straightforward to estimate mean flow properties, such as depth profiles of mean current speed and direction, from ADCP measurements (Lu and Lueck, 1999a), but calculating properties relating to phenomena that take place on smaller spatial scales than the beam spread of the ADCP is more challenging. A variety of techniques are available to estimate turbulence and wave quantities from ADCPs or similar acoustic devices (Boufferrouk et al., 2016; McMillan and Hay, 2017; Guerra and Thomson, 2017); in the current paper, we focus on the estimation of turbulent kinetic energy (TKE) using the variance method (Stacey et al., 1999; Lu and Lueck, 1999b).

An important shortcoming of the variance method for estimation of TKE is that, since it is based on measurements of velocity variance, it implicitly assumes that all velocity variance is attributable to turbulent

action. Any source of velocity variance other than the turbulence will therefore introduce a positive bias into the estimate of TKE from ADCP measurements. Most significantly, this includes the variance associated with orbital wave velocities: the bias introduced by this may be so high that a naive estimate of TKE can be approximately an order of magnitude higher than the true value. The relative importance of waves and turbulence for a given TEC will differ depending on its design; most significantly, whether it is affixed to the bed or is mounted on a floating hull. We therefore wish to be able to separately measure the effects of waves and turbulence at an energetic tidal site.

Although we propose a novel approach in this paper, the problem of disentangling waves and turbulence has been addressed previously, usually through either adaptive filtering (AF) or cospectral fitting (CF). The basis of AF is the assumption that wave motions have a larger vertical length-scale than turbulent motions. If this assumption holds, then it is possible to choose two heights in the water column with a suitable vertical separation, and compare simultaneous velocity measurements: the coherent portion of the two velocity time series is then attributable to wave motion, and the remainder to turbulent motion (Trowbridge, 1998). Although some implementations of AF required vertically separated point measurements of multiple velocity components from an array of ADVs (Shaw and Trowbridge, 2001; Feddersen and Williams

<sup>\*</sup> Corresponding author.

E-mail address: [M.Togneri@swansea.ac.uk](mailto:M.Togneri@swansea.ac.uk) (M. Togneri).

III, 2007), subsequent developments showed that the method could be successfully adapted for ADCP measurements (Rosman et al., 2008). The AF method has previously been used at sites that are significantly shallower, with weaker currents, than the site investigated here (see Section 2.1). This means that for this site, vertical lengthscales of the turbulence will be larger (as they are less constrained by the vertical boundaries), and the separation between wave and turbulent vertical lengthscales will be more difficult to maintain, meaning that the AF method will have greater trouble decoupling wave and turbulent motions.

The CF method, similarly, relies on a separation between wave and turbulent lengthscales; here, the assumption is that this will mean certain spectral features corresponding solely to waves or turbulence are clearly distinguishable in the cospectra of the total velocity record (Kirincich et al., 2010). Fitting a wavenumber-limited subrange of the observed cospectrum to a suitable semi-empirical model cospectrum of turbulence alone (more strictly, the fit is between the Ogive curve of the cospectra rather than the cospectra themselves) then allows the wave and turbulent contributions to the total velocity record to be disentangled. This method proved quite successful, and frequently offered more reliable measurements than the AF method when applied to the same measurements; however, it is not always able to yield meaningful results. Across all sites studied by Kirincich and Rosman (2011), the CF method was able to decouple waves and turbulence in a maximum of 40% of data records.

Beyond the AF and CF methods for conventional ADCPs, the use of pulse-coherent Doppler methods greatly increases the spatial and temporal resolution of acoustic profiling methods (Lohrmann et al., 1990), facilitating methods such as spectral filtering in the wavenumber-frequency domain to separate wave and turbulence contributions (Veron and Melville, 1999). However, velocity measurements obtained in this way face two important practical restrictions: the spatial extent of measurements is much smaller than is possible with a broadband ADCP, and the maximum distance of measurements from the device is much smaller (Hay et al., 2008). At high-energy tidal sites, where we wish to have measurements across the entire depth span that may be occupied by a turbine, and strong currents mean that it is very difficult to position a measurement device in mid-column, these practical restrictions are highly salient.

For most data from tidal stream energy sites, then, we have a situation where our measurements simultaneously capture two different physical phenomena in a single parameter, with no *a priori* means of disentangling them on purely physical grounds. However, as noted above, the wave contribution is strongly dominant at times of significant wave activity (Togneri et al., 2017b,a). This suggests another possibility: if the spatial profiles of the wave contribution and the ‘true’ TKE are sufficiently different, then it should be possible to identify the wave contribution with a statistically significant data mode.

In this paper, we use empirical orthogonal function (EOF) analysis to find the data modes, and we present the results from applying this analysis to the separation of waves and turbulence from ADCP estimates of TKE in a real data set. Section 2 gives details of the data collection, and presents a short introduction to the methods of data analysis. The wave contribution to the estimated TKE can also be estimated from linear wave theory, using data from a simultaneous wave buoy deployment; a brief discussion of the wave theory is given in Section 2.3. In Section 3 we present the key findings from the example data set and discuss the differences between the results from the EOF analysis and those predicted by wave theory. In Section 4 we assess the usefulness of the method, and highlight its key strengths and weaknesses; finally, we present a brief summary and conclusion in Section 5.

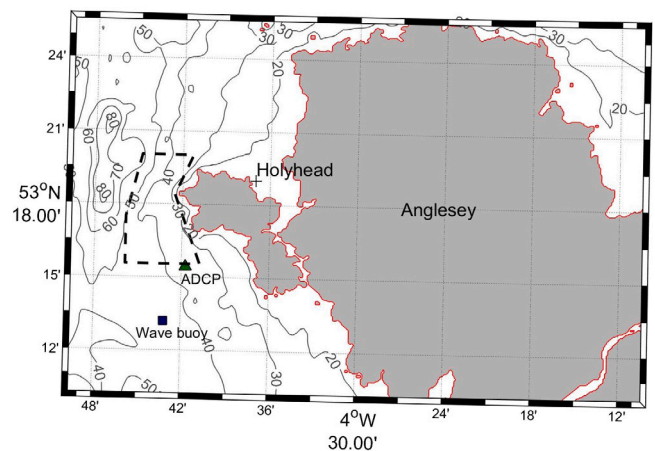


Fig. 1. Location of the ADCP and wave buoy relative to the MDZ, whose boundary is shown as a dashed line. Bathymetry contours show depth relative to mean sea level. Source: Image credit: S. Neill.

## 2. Methods

### 2.1. Instrumentation and deployment

The data used in this study is taken from a measurement campaign carried out in the Morlais Demonstration Zone (MDZ) off the coast of Anglesey in Wales. We use measurements from an RDI Sentinel V ADCP deployed on the southern edge of the MDZ (see Fig. 1) between 19/09/14 and 19/11/14. In addition to this ADCP, there are also measurements from a WaveRider buoy whose deployment period fully overlaps that of the ADCP. This buoy was located approximately 2 km to the south of the MDZ. Peak spring depth range at the ADCP deployment location was approximately 5 m (41.1–46.2 m), and the depth-averaged peak spring current was  $2.5 \text{ ms}^{-1}$ .

The ADCP measured a 15-min burst of data every hour at a sample rate of 2 Hz; the ping frequency was 614.4 kHz. For all time series presented in the rest of this paper, each burst is represented by a single time step which is calculated using all data from that burst. The vertical bin size was 0.6 m and the vertical blanking distance from the transceiver was 1.89 m; the beam angle was  $25^\circ$  from vertical. Where wave buoy measurements are compared to ADCP data from a particular burst, they are represented by an average across the same 15-min period. More details of the site and data collection can be found in Lewis et al. (2015), Piano et al. (2015).

### 2.2. Estimation of TKE from ADCP data

Heretofore we have referred to the parameter that we estimate in this study as the TKE; more precisely, the quantity estimated is the specific TKE, or TKE per unit mass. This is denoted  $k$  and is related to the Cartesian velocity components ( $u, v, w$ ) as:

$$k = \frac{1}{2} (\langle u'^2 \rangle + \langle v'^2 \rangle + \langle w'^2 \rangle), \quad (1)$$

where angle brackets denote a time average over a burst and a prime denotes the fluctuation component.

Although the Sentinel V has five beams (one vertical and four off-vertical), following the work presented in Togneri et al. (2017a) we note that using the fifth beam does not significantly alter the estimated values of TKE, and introduces greater uncertainty. Thus, we use the conventional four-beam estimate of TKE using the variance method throughout this study. A detailed description of the variance method for estimation of TKE can be found in e.g., Stacey et al. (1999) or Lu and Lueck (1999b), so we do not propose to describe the method in depth in the current paper. In short, if we take the velocity measured

along the  $i$ th beam to be  $b_i$ , then we can express its variance as  $\langle b_i'^2 \rangle$ . By assuming that the second-order statistics of the turbulence across the beam spread of the ADCP are spatially uniform, and that they are approximately stationary over the averaging period, it can be shown that the ADCP can estimate TKE as:

$$k = \frac{\sum_{i=1}^4 \langle b_i'^2 \rangle}{4 \sin^2 \theta (1 - \xi (1 - \cot^2 \theta))}, \quad (2)$$

where  $\theta$  is the inclination angle of the off-vertical beams and  $\xi$  parametrises the turbulent anisotropy. We use a value of  $\xi = 0.1684$ , following the semi-empirical analysis of open-channel flows by Nezu and Nakagawa (1993).

Because Eq. (2) involves only addition of beam variances, we can be sure that the effect of Doppler noise is a positive bias on each beam's contribution to the calculated  $k$  value; this makes it quite straightforward to find a conservative estimate of the bias due to instrument noise. A detailed description of the noise correction method is given in Togneri et al. (2017b); an overview of the TKE calculated using this method and corrected for noise bias is shown in Fig. 2. Calculating the variance of the  $k$  value is less straightforward, as Eq. (2) yields a single  $k$  value for each burst. We therefore estimate the variance of  $k$  for a given burst by bootstrapping the variance of  $\langle b_i'^2 \rangle$  for each beam, and then combining these 'variances of variances' to estimate the variance of  $k$  under the assumption that  $\text{Var}(\langle b_i'^2 \rangle)$  and  $\text{Var}(\langle b_j'^2 \rangle)$  are uncorrelated  $\forall i \neq j$ .

The estimate of  $k$  in Eq. (2) assumes a given relationship between the alignment of the beams and the directions of the wave velocities. If the ADCP is tilted from the vertical (due to, for instance, a sloping seabed) however, then this relationship does not necessarily hold. Following the approach of Lu and Lueck (1999b), further developed in Rosman et al. (2008), we suppose that the ADCP tilt may be characterised by a pitch angle  $\phi_P$  about the axis on which beams 1 and 2 lie, and a roll angle  $\phi_R$  about the axis on which beams 3 and 4 lie. We can then relate the vector of device-centric velocities ( $u^\dagger, v^\dagger, w^\dagger$ ) to the vector of earth-centric velocities ( $u, v, w$ ) with a simple linearised rotation:

$$\begin{bmatrix} u^\dagger \\ v^\dagger \\ w^\dagger \end{bmatrix} = \begin{bmatrix} 1 & 0 & -\phi_R \\ 0 & 1 & \phi_P \\ \phi_R & -\phi_P & 1 \end{bmatrix} \begin{bmatrix} u \\ v \\ w \end{bmatrix} \quad (3)$$

In this case, using a sum of beam variances to estimate  $k$ , as in Eq. (2), will not give exactly  $k$  but rather  $k$  plus some error terms associated with the tilt. Thus, the equation should be rendered as:

$$\frac{\sum_{i=1}^4 \langle b_i'^2 \rangle}{4 \sin^2 \theta (1 - \xi (1 - \cot^2 \theta))} = \frac{1}{2} (\langle u'^2 \rangle + \langle v'^2 \rangle + \langle w'^2 \rangle),$$

and by substituting in the appropriate expressions for ( $u^\dagger, v^\dagger, w^\dagger$ ) from Eq. (3), we find that for an ADCP with tilt:

$$\frac{\sum_{i=1}^4 \langle b_i'^2 \rangle}{4 \sin^2 \theta (1 - \xi (1 - \cot^2 \theta))} = \frac{1}{2} (\langle (1 + \phi_R^2) u'^2 \rangle + (1 + \phi_P^2) \langle v'^2 \rangle + (1 + \phi_P^2 + \phi_R^2) \langle w'^2 \rangle - 2\phi_P \phi_R \langle u' v' \rangle) \quad (4)$$

The additional terms due to tilt are all second order with respect to the tilt angles; the error that they will introduce is therefore below 1% as long as tilt angles remain under  $5.7^\circ$ . Approximately 1.2% of measurements were found to fail this criterion; by excluding data from these times when calculating the beam variances, we can be confident that tilt bias in the  $k$  estimate is minimal.

As noted in Section 1, this method produces an estimate of  $k$  which assumes that all variance in the beam velocities is due to turbulent fluctuations. If wave action, or some other non-turbulent phenomenon, generates additional velocity variation, the estimated quantity  $k$  will not correspond to TKE but will capture contributions from both turbulence and waves. To clarify this distinction, in the remainder of the paper, we denote the estimate obtained using Eq. (2) as  $k_{ADCP}$ . Under

the assumption that the waves and turbulence are not statistically correlated (cf. for instance the analysis of Anis and Moum, 1995), their contributions to  $k_{ADCP}$  can be regarded as superposed on one another, and we can simply regard the estimate as a sum of turbulent and wave contributions:

$$k_{ADCP} = k_t + k_w. \quad (5)$$

In this formulation,  $k_t$  is the true TKE, and  $k_w$  is a 'pseudo-TKE' associated with wave orbital velocities that causes an upwards bias in the ADCP estimate of TKE.

### 2.3. Velocity variance in linear wave theory

From Airy wave theory, wave orbital velocities in the presence of significant mean currents are the spatial derivatives of the velocity potential function:

$$\varphi(x, z, t) = \frac{\sigma}{\kappa} a \frac{\cosh(\kappa(z+h))}{\sinh(\kappa h)} \sin(\kappa x - \omega t) \quad (6)$$

Here,  $x$  and  $z$  express horizontal and vertical spatial position (recall that  $z$  is defined as displacement down from the surface),  $t$  is time,  $a$  is wave amplitude,  $\kappa$  is wavenumber, and  $\omega$  and  $\sigma$  are observed and intrinsic frequency respectively. On this basis, the expected pseudo-TKE from wave velocities for an averaging period sufficiently long compared to the wave period will be:

$$k_w = \frac{1}{4} \frac{\sigma^2 a^2}{\sinh^2(\kappa h)} \sinh^2(\kappa(z+h)) \quad (7)$$

The parameters  $a, \kappa, \omega$  and  $\sigma$  can be obtained from the wave buoy. Of these, the wave buoy only directly measures observed frequency  $\omega$ , although it also provides the significant wave height, which is divided in half to yield wave amplitude  $a$ . To calculate  $\kappa$ , we take the observed frequency  $\omega$ , along with the ADCP's measurements of water depth  $z$  and surface current speed  $U$  and the angle  $\theta$  between wave and current direction; these are then used in the dispersion relation:

$$(\omega - \kappa U \cos \theta)^2 = g \kappa \tanh(\kappa z), \quad (8)$$

which can be solved iteratively for  $\kappa$  (cf. the procedure described in Wolf and Prandle, 1999). It is then trivial to calculate  $\sigma$ . This gives us all the data needed to fully specify the expected pseudo-TKE profiles due to linear waves, as given in Eq. (7). Note that strictly Eq. (8) is only correct where the current velocity  $U$  is uniform in depth. Analysis of the longitudinal velocity profile in the at this site shows that for floods, there is no more than a 5% difference in maximum and minimum velocity in the top 20 m of the measurable portion of the water column; for ebbs, this figure is 17 m.

### 2.4. EOF analysis

EOFs are a well-established technique for analysing climatic and meteorological data; mathematically equivalent techniques such as proper orthogonal decomposition (POD) or principal component analysis (PCA) are also widely applied for identifying or isolating specific features within flow fields where multiple phenomena are acting simultaneously (Clavero et al., 2016; Scherl et al., 2020). Björnsson and Venegas (1997) is a very good introduction to the method for readers not familiar with the technique; there are also more comprehensive texts describing EOF analysis in greater detail (Preisendorfer, 1988; Jolliffe, 2011). In brief, EOF analysis decomposes a zero-mean spatiotemporal dataset into a spatial basis (the members of this basis are the empirical orthogonal functions from which the method takes its name), which can be combined linearly with time-dependent weightings to reconstruct the original dataset. The weight of each basis function at a given time is specified by the time-varying "expansion coefficient". In general, if we have some spatiotemporal dataset  $D(\mathbf{x}, t)$  that is decomposed into  $N$  basis functions  $\text{EOF}_i(\mathbf{x})$  and expansion

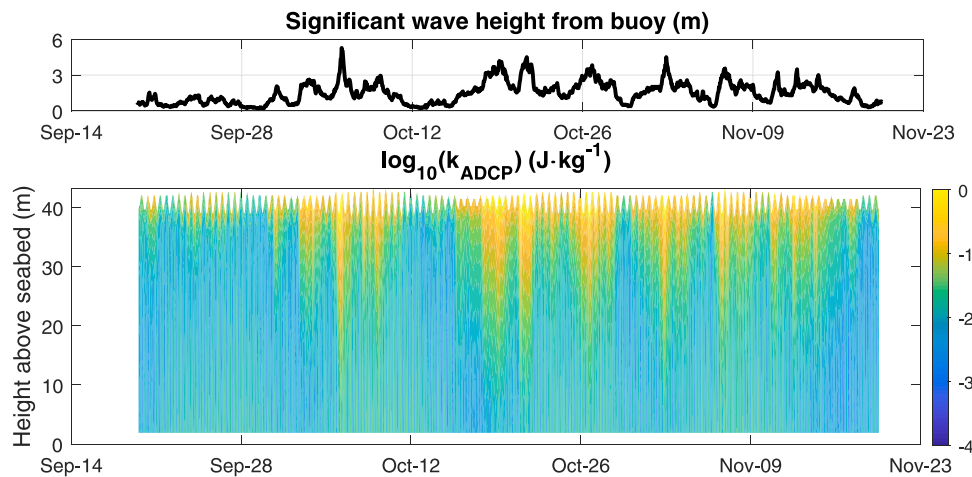


Fig. 2. Bottom panel shows pseudo-TKE as estimated from ADCP data using Eq. (2) for the whole deployment. Top panel shows the concurrent buoy measurements of significant wave height. (For interpretation of the references to color in this figure legend, the reader is referred to the web version of this article.)  
Source: Figure adapted from Togneri et al. (2017b).

coefficients  $EC_i(t)$ , with  $i = 1, \dots, N$ , then the original data can be fully reconstructed as:

$$D(\mathbf{x}, t) = \sum_{i=1}^N EOF_i(\mathbf{x}) \times EC_i(t). \quad (9)$$

Here  $N$  is the number of points in the spatial grid. (In this study,  $N$  is 62 i.e., the number of bins in the ADCP profiles of estimated TKE.) By ordering the EOFs by the magnitude of their contribution to the total variability of  $D$ , it is possible to pick out the most significant data modes from the overall dataset and attempt to identify them with particular physical phenomena. As the wave contribution to total pseudo-TKE is seen to significantly dominate the turbulence contribution at times of strong wave activity, we expect that the first EOF will correspond almost entirely to wave action. If this is indeed the case, then the value of  $EC_1(t)$  will indicate whether wave-generated pseudo-TKE is a significant contribution to  $k_{ADCP}$  at time  $t$ : a high positive value will indicate that waves are acting to positively bias the ADCP estimate of TKE, while a low or negative value will indicate that wave action is negligible.

As mentioned at the start of this section, EOF analysis is only able to work with a data set whose time mean is zero, so we discard the mean before beginning the analysis, and then re-add it when reconstructing the decoupled wave and turbulent components. However, because TKE is always positive, the wave pseudo-TKE will also bias the mean value of  $k_{ADCP}$  high. To fully capture the wave contribution, we must have an estimate of this mean bias as well as the time-varying component from EOF analysis. To facilitate this we recast Eq. (5) in terms of the mean and time-varying contribution from waves and turbulence as:

$$k_{ADCP} = \overline{k_{ADCP}} + \widetilde{k_{ADCP}} \\ = (\overline{k_t} + \widetilde{k_t}) + (\overline{k_w} + \widetilde{k_w}) \quad (10)$$

Here, an overbar indicates a mean value and a tilde indicates the time-varying component. These apply over the whole two-month dataset, cf. the  $\langle \cdot \rangle$  and  $\prime$  notation which were applied to data within a single 15-min burst in Eqs. (1) and (2). Thus, we anticipate a non-zero value of  $\overline{k_w}$  for the mean wave bias across the whole dataset, even although at times of low wave action  $k_w$  will be instantaneously zero.

If the EOF approach outlined above is correct, then  $EOF_1(\mathbf{x}) \times EC_1(t) \approx \widetilde{k_w}$ . However, we still need an estimate of the wave mean bias  $\overline{k_w}$  if we are to fully separate waves and turbulence. We achieve this by assuming that the first EOF does indeed capture the variability of wave-generated pseudo-TKE. If this is the case, then  $EC_1(t) < 0$  corresponds to times when wave action is not significant. A mean profile of  $k_{ADCP}$  calculated from a subsample containing only these times will then be

equal to  $\overline{k_t}$ , and we can then calculate  $\overline{k_w} = \overline{k_{ADCP}} - \overline{k_t}$ . If we are able to verify that the  $\overline{k_t}$  profile found in this way is correct, then we can in principle affirm the correctness of the assumption that the first EOF can be identified with  $\widetilde{k_w}$ . This then allows us to separate out all four components on the right-hand side of Eq. (10).

The EOF method requires a dataset in which the spatial points are the same for each timestep; since the water depth changes throughout the cycle we must truncate the data prior to carrying out the EOF analysis. We elect to do this by truncating downwards from the highest point in the water column containing valid data, such that each successive burst contains the same depth range relative to the surface. This choice is made on the grounds that wave action extends downwards through the water column, so defining the data set such that its location relative to the point of maximum wave activity is fixed will make the EOF analysis more likely to pick out modes that correspond to genuine wave phenomena. Once  $k_w$  has been identified and subtracted from  $k_{ADCP}$ , the remainder, which should be due solely to turbulent action, can then be re-analysed taking the seabed as zero. The highest point in the water column from which data is available is constrained by the effects of sidelobe interference, which means very near the surface strong echoes from the water–air boundary make accurate measurement impossible (Appell et al., 1991; Nystrom et al., 2007). For the inclination angle of  $25^\circ$  in the ADCP used in this study, this means that measurements from the uppermost 6.6% of the water column do not yield useful data.

### 3. Results

Fig. 2 gives an overview of the whole dataset, by showing the distribution of the ADCP estimate of TKE across all water depths for the complete deployment period and comparing it to the depth-mean current velocity and buoy measurements of significant wave height during the same period. There is a clear coincidence of high waves and high values of  $k_{ADCP}$  near the surface (up to magnitudes of approximately  $1 \text{ m}^2 \text{ s}^{-2}$ , cf. the values around  $1 - 5 \times 10^{-2}$  seen in studies at other tidal sites such as that by Milne et al. (2017)); this indicates that, as proposed in Sections 1 and 2, the most significant statistical mode is likely to be strongly correlated with wave action. We can further demonstrate how strongly the waves dominate the turbulence by examining a sample spectrum of along-beam velocities. A PSD of the velocity measured along the direction of beam 1 for a burst near the start of the deployment period, which is not a period of particularly strong wave activity (cf. Fig. 2) is given in Fig. 3; this clearly shows the extent to which the energy associated with wave action dominates the PSD, as the wave peak is by orders of magnitude the most significant feature.

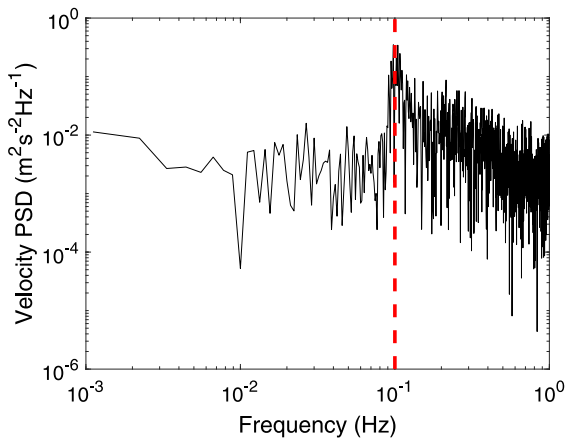


Fig. 3. PSD of along-beam velocity for beam 1 for the burst starting at 1300 on 19/09/14, near the start of the deployment period. The PSD presented is depth-averaged over the top quartile of the portion of the water column sampled by the ADCP. Red dashed line indicates the modal wave period measured by the wave buoy during the same time.

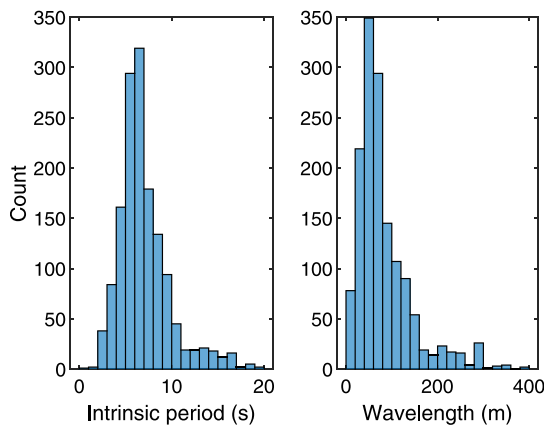


Fig. 4. Distributions of wave period and wavelength calculated from buoy measurements for the ADCP deployment period.

### 3.1. Observed wave properties

Fig. 4 shows the probability distributions of the intrinsic wave period and the wavelength from all 15-min bursts across the duration of the ADCP deployment, as measured with the wave buoy. These distributions are sharply peaked — quantitatively, the kurtosis of the period distribution is 5.99 and that of the wavelength distribution is 7.43. Most wave observations have a period in the range  $6.5 \pm 1.4$  s and a wavelength in the range  $65 \pm 26$  m. Certain key effects of the wave-current interaction on the relationship between observed frequency  $\omega$  and intrinsic frequency  $\sigma$  are detailed in the data in Fig. 5; panel a shows that the scatter remains clustered around unity for all observations. Panels b and c show that the difference between  $\omega$  and  $\kappa$  behaves as expected with respect to the properties of the currents and waves: a greater current speed generally tends to produce a greater discrepancy; the simple best-fit linear relationship indicated by the black line in panel b has an  $R^2$  of 0.42. Additionally, as the angle between wave and current directions gets closer to orthogonal (i.e.,  $\pi/2$ ), the difference between  $\omega$  and  $\sigma$  shrinks.

### 3.2. EOF analysis

Turning to the performance of the EOF analysis, we can estimate the relative importance of an EOF mode by its normalised eigenvalue, i.e., its own eigenvalue divided by the sum of all eigenvalues. This gives a measure of the proportion of total variance in the dataset explained by a particular data mode. For our dataset, the first EOF mode explains 97.1% of the overall variance; given the apparent strong dominance of the wave pseudo-TKE, as seen in contour plot of Fig. 2, this is consistent with the first statistical mode corresponding approximately to the wave action.

Recall, as per the discussion in Section 2.4, that although we hope to capture the time-varying component of the wave pseudo-TKE with EOF analysis, we must take a different approach to finding the wave-associated bias in the mean value of  $k_{ADCP}$ . In Fig. 6 we examine the decomposition of the time-mean portion  $\overline{k_{ADCP}}$  of the total measured pseudo-TKE, as proposed in Section 2.4 and summarised by Eq. (10). We can see that filtering the profile of mean  $k_{ADCP}$  by the proposed low-wave criterion (i.e.,  $EC_1(t) < 0$ ) has yielded an estimated  $\overline{k_w}$  profile that is a good approximation to a  $\sinh^2$  function, as we would expect from Eq. (7). The  $\overline{k_t}$  profile is mostly constant in the lower part of the water column, at depths greater than ca. 18 m below the

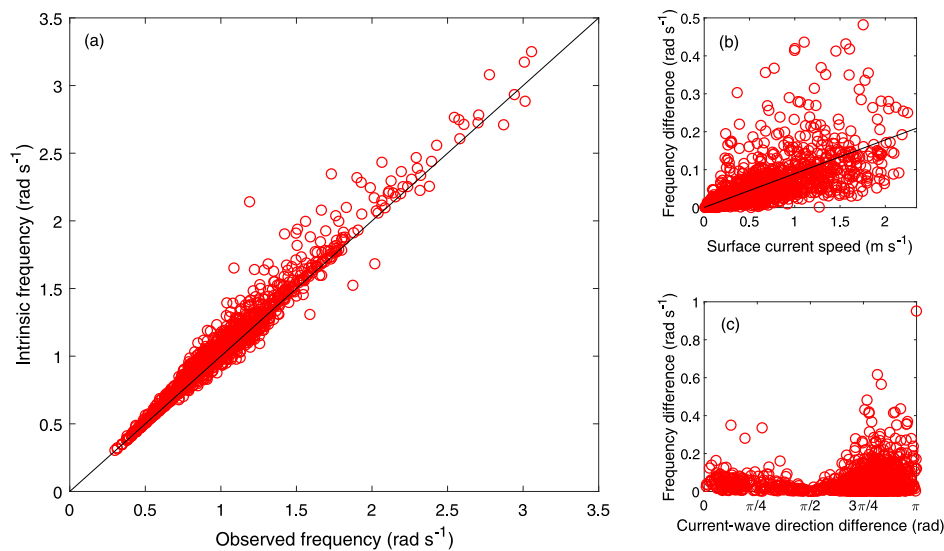


Fig. 5. Scatter plot of observed vs. intrinsic frequency for each burst from wave buoy observations (panel a); the dependence of the difference on the surface current speed and the directional mismatch between surface current and waves is shown in panels b and c respectively.

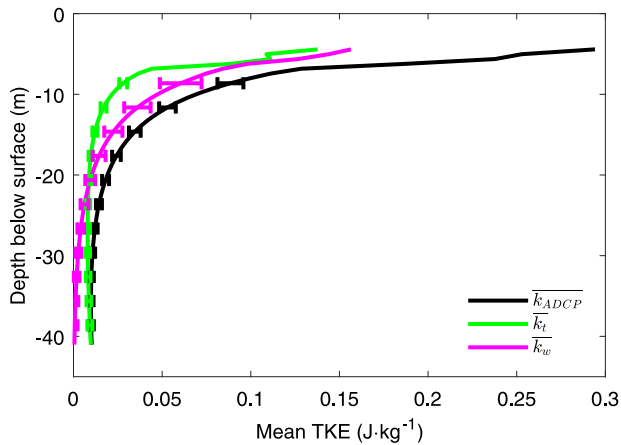


Fig. 6. Time-mean profile of the ADCP estimate of TKE across entire measurement period, and its components due to wave and turbulent action, estimated using the method described in Section 2.4. Error bars indicate the 95% confidence interval (i.e. twice the standard deviation), calculated by bootstrapping of the variance as described in Section 2.2.

surface. We see no peak in  $k$  near the bed, although this may be simply because the expected near-bed increase occurs below the lowest measurement point. However, close to the surface of the water, in a depth range roughly between 5–18 m, the profile exhibits an approximately exponential behaviour. This suggests that the EOF analysis has not completely removed the wave pseudo-TKE from the estimate of  $k_t$ ; in Section 4 we demonstrate a correlation between the near-surface maximum in  $k_t$  and wind action, indicating that wind waves may be a significant contributor to  $k_t$  near the surface. We can also see that the estimated variability of  $k_w$  is higher than the estimated variability of the profile of mean TKE when using all bursts,  $k_{ADCP}$ ; this is consistent with wave action being the phenomenon driving velocity variability in excess of that associated with turbulent fluctuations.

### 3.3. Comparison of observations and EOF

To examine how the EOF analysis prediction of pseudo-TKE compares with the observed wave properties throughout the measurement period, Fig. 7 compares the significant wave height with estimates of wave-generated pseudo-TKE  $k_w$  from the EOF method and from Airy wave theory at a depth slightly below the surface. It is apparent that all three of the time series shown in the figure track one another quite closely. This correlation is quantitatively very good; the Pearson correlation coefficient for any pair of these three variables is in the range 0.94–0.96. We can get a more holistic assessment of the agreement between the two different estimates of wave pseudo-TKE by examining

the depth-mean error between the estimates, as shown in Fig. 8. The absolute error is not large, but it is clear that the relative error can become very high. This is simply due to the fact that both estimates can take very small values, resulting in extremely high spikes in the relative error. The exact timing of the spikes depends on whether the relative error is calculated with the EOF estimate or the linear theory estimate on the denominator. A simple time average of the relative error between the two estimation methods is very high (on the order of  $10^2 - 10^4\%$ ) due to these spikes, although in Section 4 we argue that a more meaningful estimate of the error is 37.0%.

Finally, in Fig. 9, we show the result of using EOF analysis to decompose the total ADCP estimate of TKE,  $k_{ADCP}$ , into the ‘true’ turbulent kinetic energy  $k_t$  and the wave-generated pseudo-TKE  $k_w$ . The two panels of this figure correspond to the same  $k_{ADCP}$  dataset plotted in the bottom panel of Fig. 2 broken into wave and turbulent components according to the simple decomposition of Eq. (5) i.e., summing the datasets shown in these two panels will perfectly recover the initial estimate. The  $\log_{10}$  of each value has been used to generate the contour plot, as this allows us to see the difference in magnitude between the  $k_w$  and  $k_t$  components while still preserving the visibility of the smaller variations in value. At several points, one or the other of the components takes a value below zero. This is not physically meaningful, but is instead an artefact of the decomposition method when a particular contribution is negligibly small: at such times, the random error between the statistical decomposition and the underlying physical contributions of the waves and turbulence can take a value larger than the true, negligibly small, value. If this error is negative, then the EOF-estimated value of  $k_w$  or  $k_t$  can go below zero. Note that as the EOF decomposition technique uses a subset of the total data that is a constant depth range, with reference to the surface, this leaves a variable number of depth bins near the seabed untreated by this analysis; we deal with these by assuming that the wave contribution is negligible at this point and setting  $k_t = k_{ADCP}$  for these few near-bed bins.

Using the log scale for plotting  $k_t$  makes it easy to see the diurnal variation and the spring–neap cycle in the upper panel of Fig. 9 (note the four broad peaks in value near the bed centred around 28th September, 12th and 26th October, and 9th November). It is also clear that no similar time variation is visible in the  $k_w$  plot. This is a strong indication that the separation has genuinely found a way of decomposing the data set into two components which are mostly identifiable with turbulence and waves. However, there are still some aspects of the separation that are less satisfactory. Near the surface, the  $k_t$  estimate still shows a significant peak (as we might expect based on the mean profile shown in Fig. 6), and there are a few anomalous transient features (e.g., around 5th October) which may be wave-related. We discuss some possibilities for the causes of these discrepancies, and ways they might be addressed, in the following section.

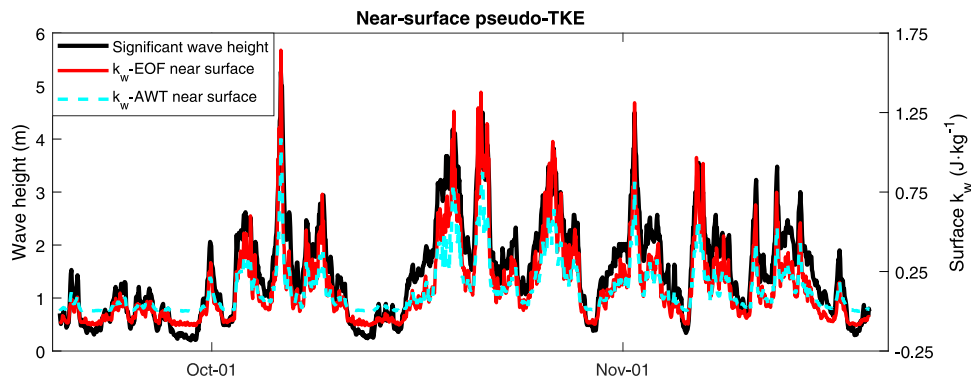


Fig. 7. Comparison of significant wave height as measured from buoy (scale on left axis) with wave-generated pseudo-TKE estimated using EOF analysis ( $k_w$  – EOF) and using Airy wave theory ( $k_w$  – AWT) (scale on right axis).

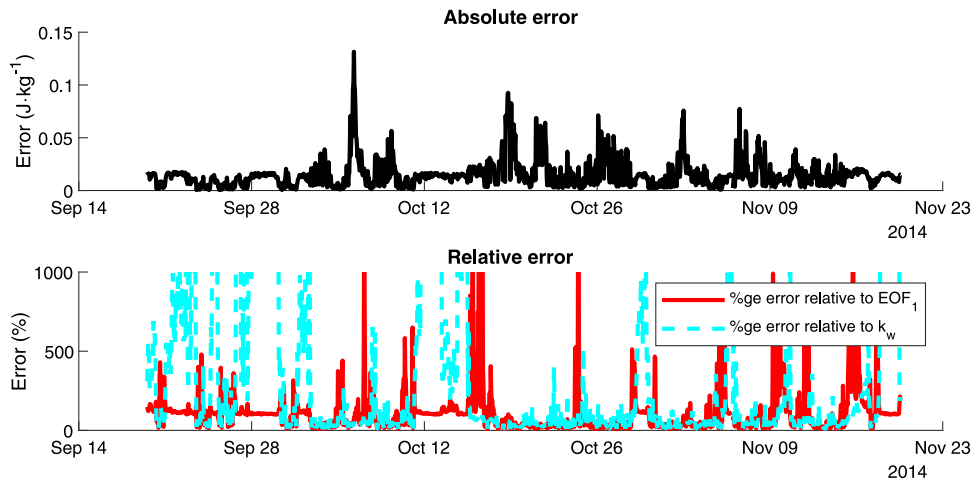


Fig. 8. Overview of error between the EOF and linear theory estimates of wave-generated pseudo-TKE, throughout the entire measurement period. Top panel shows the mean absolute error (in  $J \cdot kg^{-1}$ ) throughout the whole measured depth; bottom panel shows the relative error as a percentage.

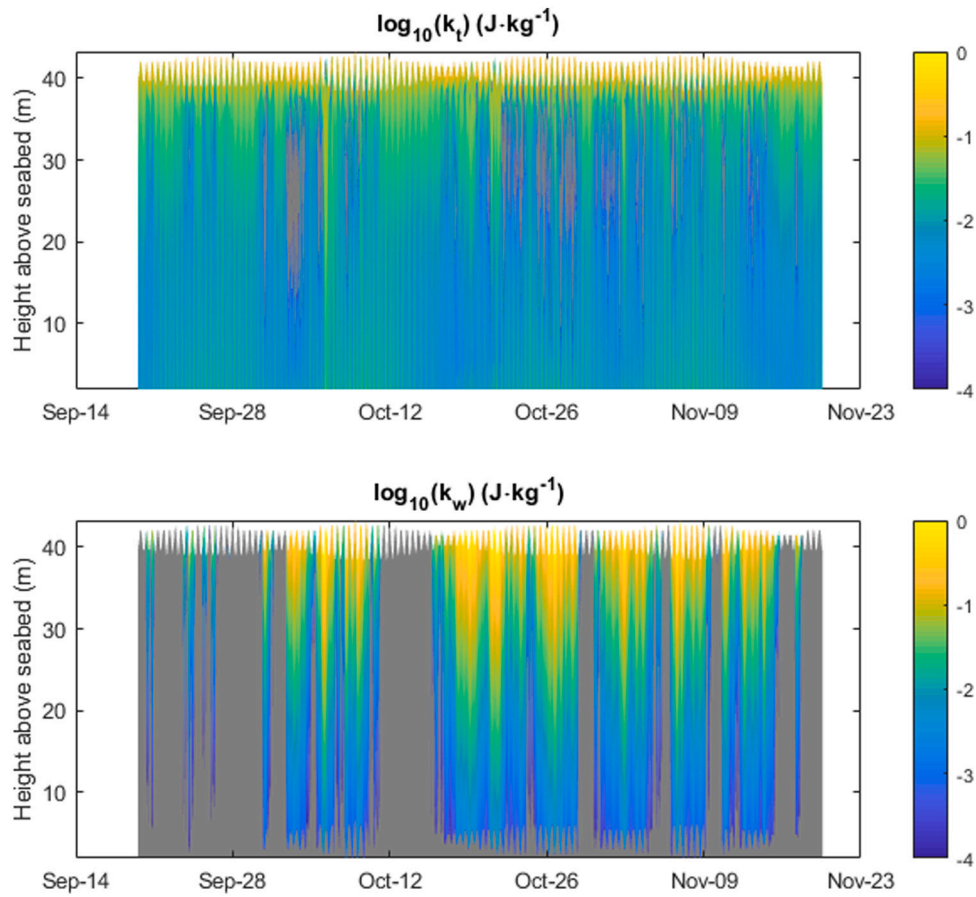


Fig. 9. Separation of the measured  $k_{ADCP}$  (cf. Fig. 2, bottom panel) into turbulent ( $k_t$ ) and wave ( $k_w$ ) contributions, using a single EOF mode. The colour map used for the plots is derived from the  $\log_{10}$  values of the contributions. Values below zero in either component are shown in grey. (For interpretation of the references to color in this figure legend, the reader is referred to the web version of this article.)

#### 4. Discussion

We have seen in Fig. 8 that, although the absolute error between the EOF and theory estimates of  $k_w$  may be quite small, the relative error can become very large. On the face of it, this suggests that poor agreement between EOF and theory; however, to better understand the importance of these very large relative errors, it is instructive to examine the relationships between the error and other flow parameters.

The size of the absolute error between estimates of  $k_w$  is important to understand the behaviour of the corresponding relative error. In Fig. 10, we show how the absolute error depends on key wave parameters, and on the near-surface value of the estimated pseudo-TKE itself. The relationships between error and wave period or wavelength are not immediately apparent, but the peak errors in panels (a) and (c) approximately coincide with the most energetic wave conditions. The dependence of absolute error on wave height is more straightforward:

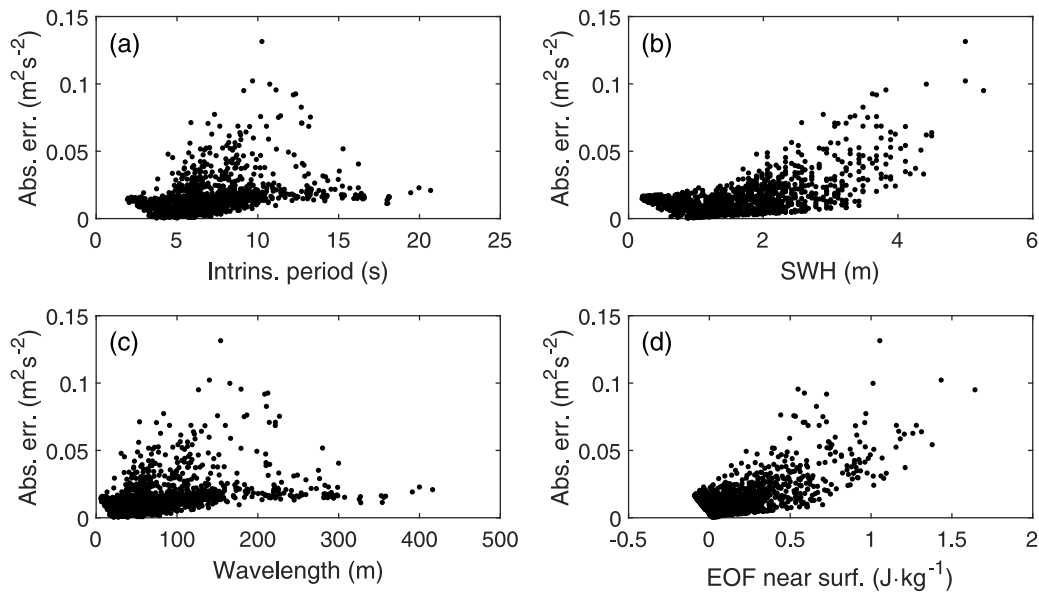


Fig. 10. Dependence of absolute error (in  $\text{J kg}^{-1}$ ) on (a) intrinsic wave period (b) significant wave height (c) wavelength (d) EOF estimate of near-surface wave pseudo-TKE.

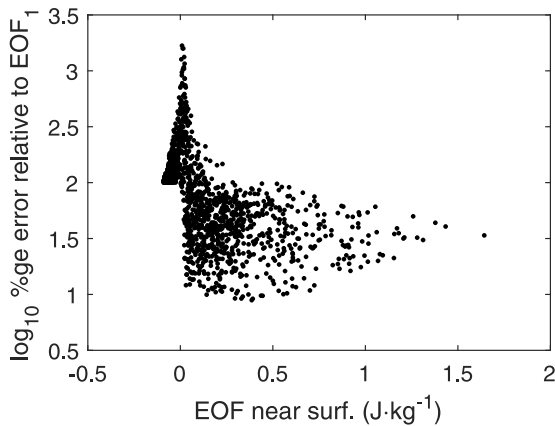


Fig. 11. Dependence of relative error on EOF estimate of near-surface wave pseudo-TKE.

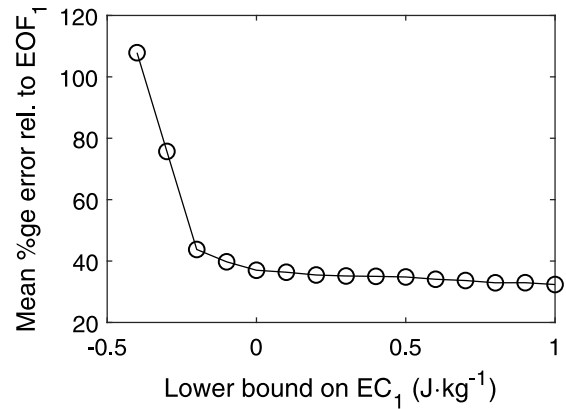


Fig. 12. Effect on mean relative error of filtering bursts by excluding those below a certain  $EC_1$  limit.

panel (b) shows an approximately quadratic relationship between error and significant wave height (cf. the wave amplitude term in (7)). Most simple, however, is the approximately linear relationship between error and near-surface pseudo-TKE. For the EOF-based estimate used in panel (d), the correlation is  $R = 0.63$ ; we do not show the relationship with the linear theory estimate as it is very similar, but the correlation in that case is even stronger ( $R = 0.70$ ).

These results should be borne in mind when interpreting the behaviour of the relative error as seen in Fig. 11. This shows a very high peak in relative error, on the order of 1000%; in other words, it shows that the EOF estimate of wave pseudo-TKE and the linear theory predictions are often different by approximately an order of magnitude. This is not *prima facie* evidence that the EOF analysis is a good means to estimate wave pseudo-TKE; however, it is clear that these very high errors occur only when the EOF estimate of wave pseudo-TKE is near zero. Comparing this to panel (d) of Fig. 10, we see that the absolute error for such bursts is not behaving unusually, and that therefore the spike in relative error is purely due to very small values of the denominator in the calculation rather than any true divergence in the absolute values of the two pseudo-TKE estimators.

This means that attempts to calculate  $k_w$  from theory or by EOF analysis are only robust when the wave pseudo-TKE is, in some sense,

sufficiently large; otherwise, the estimates provided by these methods may be erroneous or unhelpful. By a robust estimate of  $k_w$  we mean one that can be well-corroborated between the two methods. For this to be meaningful, however, we must be able to more precisely define a ‘sufficiently large’ pseudo-TKE. If we assume that a very high relative error between the two estimation methods indicates a time at which both methods are returning a poor estimate of  $k_w$ , then we can consider a criterion for selecting good estimates that uses the value of this error as a measure of goodness.

This selection criterion should ideally be possible to choose *a priori*, without knowledge of the error. Bearing this constraint in mind, the most intuitive choice is to say that suitable estimates of  $k_w$  are only obtained when the expansion coefficient of the first EOF mode of the  $k_{ADCP}$  data set is positive i.e., when  $EC_1(t) > 0$ . Fig. 12 shows that filtering the dataset by excluding bursts whose  $EC_1$  value is below a certain threshold has a significant impact on the mean error, and that if we set this threshold to zero the mean error between the linear theory estimate of  $k_w$  and the estimate obtained using EOF analysis, the mean error is approximately 37%.

Fig. 9 shows that using EOF to decompose  $k_{ADCP}$  into its turbulent and wave components seems to be quite successful. However, there are two significant features to address:  $k_i$  values still have a peak in the

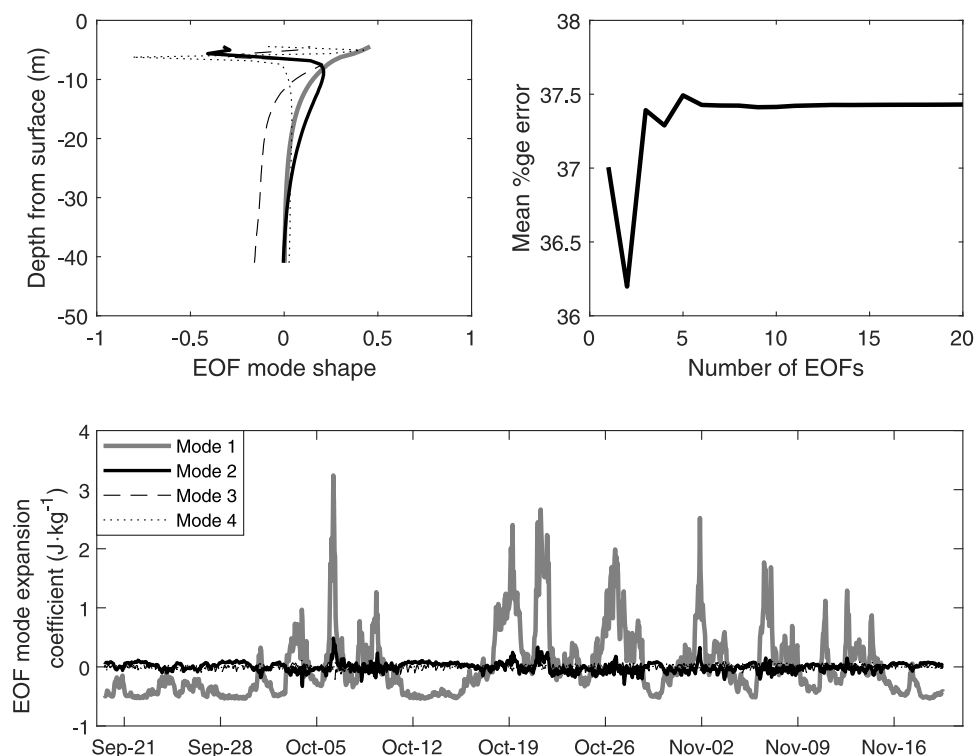


Fig. 13. Top left: comparison of normalised EOF mode shapes for the first four modes. Top right: effect on mean relative error of increasing number of modes used in EOF estimate of  $k_w$ . Bottom: comparison of expansion coefficients for the first four EOF modes across the duration of the entire record.

surface-most stations, which indicates that not all wave activity has been removed; and there are significant transient features that are not obviously associated with any tidal constituent. These may be due to the first EOF mode not capturing the whole of the wave physics: higher modes might correct these transient spikes. To investigate this possibility, we use the error criterion from above to test if the agreement between the theory estimate of  $k_w$  and the EOF estimate is improved by including more EOF modes. In terms of the simple decomposition presented in Eq. (10), this addition of modes alters how  $\widehat{k}_{ADCP}$  is split into its wave and turbulent contributions  $\widehat{k}_w$  and  $\widehat{k}_t$ , but does not affect the estimate of how waves and turbulence contribute to the estimated  $\widehat{k}_{ADCP}$ .

The results of this test, as well as a comparison of the first four EOF modes, are shown in Fig. 13: this shows that the error is indeed somewhat reduced by adding the second EOF to the first, from 37.0% to 36.2%. It is clear from the bottom panel of Fig. 13 just how dominant the first mode is; recall from Section 3 that the first mode explains approximately 97% of the total variability in the record; here we see that the second mode explains approximately 1.8% and no other mode exceeds 0.5%.

The mode shapes seen in the top left panel do not obviously correspond to a particular physical phenomenon in themselves; rather, they appear to mostly be ‘corrections’ to the first mode, mirroring its shape through most of the water column but changing sign near the surface to allow the surface-most bin to be slightly increased or decreased at a particular time. Incorporating the second mode visibly improves the decomposition, as can be seen in Fig. 14: the near-surface maximum is reduced although still present, the transient features in the single-mode decomposition are eliminated, and the mid-depth ‘patches’ where  $k_t < 0$  are significantly reduced in size. The mode shapes shown in Fig. 13 are robust to observational variance of the TKE field from which they are calculated. Recalculating the EOF modes for TKE fields at the extremes of the 95% confidence interval (cf. Fig. 6) produces very similar mode shapes, with a relative difference in magnitude for the first four mode shapes of 1.01%, 7.89%, 0.39% and 1.84% respectively.

It is possible that the near-surface maximum seen in the decomposed  $k_t$  record may be associated with shorter-period waves. This would not be picked out by the EOF analysis, which instead finds statistical modes more closely tied to long-period waves which generate pseudo-TKE throughout the measured water depth. We can test the plausibility of this explanation by comparing the near-surface estimates of  $k_t$  with wind measurements from the nearby RAF Valley weather station, and this is illustrated in Fig. 15. There is no clear correlation between the wind speed and the near-surface  $k_t$  estimate itself; however, in examining the data set we noticed that high-frequency fluctuations appeared to be much more prominent when wind speeds are higher. To investigate this, we calculated a simple rolling variance of the near-surface  $k_t$  estimate: the ‘variance’ for each burst is calculated from a window of 20 observations centred around itself. The results of this are shown in the bottom panel of this figure; a comparison of the top and bottom panels makes it clear that this rolling variance is tracking the windspeed quite closely. We are therefore confident in saying that the near-surface maximum in the  $k_t$  estimate obtained from EOF analysis is associated with wind action. Although we cannot be certain of the precise mechanism, it may be from an additional source of error in the method associated with higher uncertainties in ADCP estimates of TKE near the surface, or on the other hand it may be genuine and associated with a phenomenon such as turbulence generated by wave breaking.

## 5. Summary and conclusions

In general, both waves and turbulence act at energetic tidal sites, and both are significant environmental factors affecting TEC fatigue and reliability. It is possible to measure wave properties alone using a wave buoy, although the strong currents associated with tidal energy sites frequently cause practical problems for buoys e.g., being dragged down at the limits of their mooring. These problems may be possible to overcome with acoustic instruments incorporating a vertical beam dedicated to measuring wave properties, as previous study has shown that

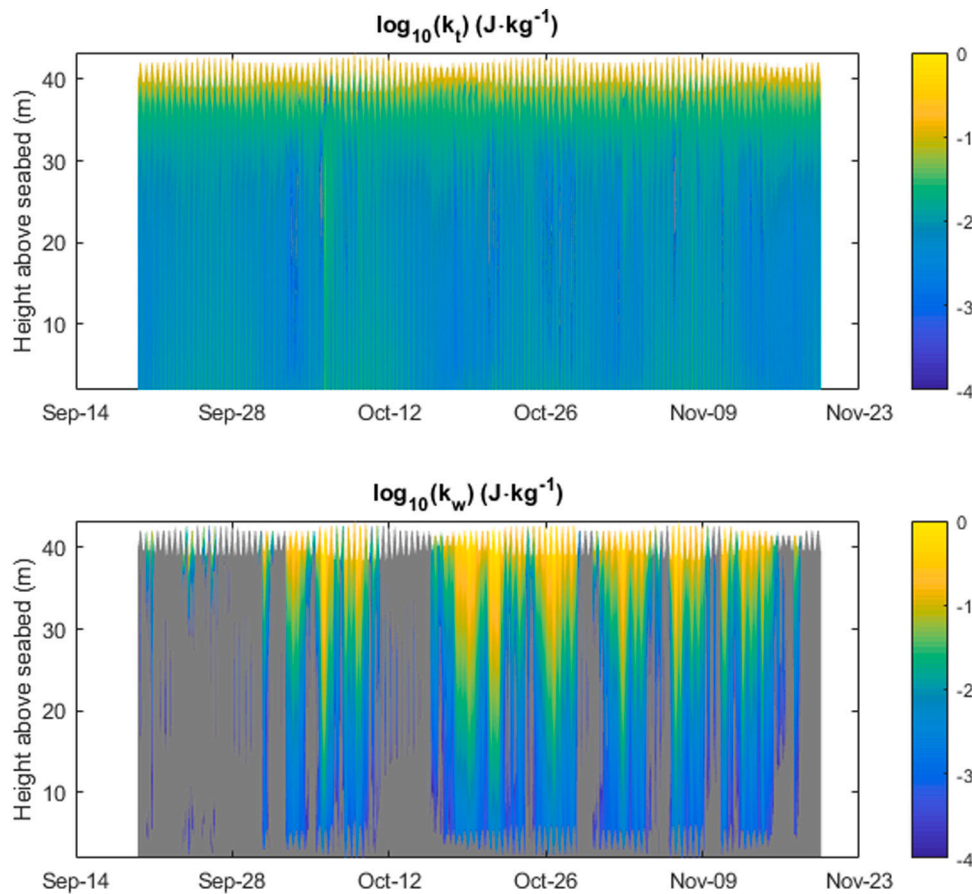


Fig. 14. Separation of the measured  $k_{ADCP}$  into turbulent ( $k_t$ ) and wave ( $k_w$ ) contributions, using the first two EOF modes. The colour map used for the plots is derived from the  $\log_{10}$  values of the contributions. Values below zero in either component are shown in grey. (For interpretation of the references to color in this figure legend, the reader is referred to the web version of this article.)

the vertical beam does not greatly improve estimates of TKE (Togneri et al., 2017a).

The bed-mounted ADCPs that are typical of site measurements (both those intended for scientific investigations and those recommended by the relevant IEC standards for industrial applications, IEC/TS 62600-201), however, face unique challenges in measuring key turbulence parameters. The measurements from these devices rely on the standard variance method, cf. Eq. (2) (Stacey et al., 1999; Lu and Lueck, 1999b), and thus, as discussed in Section 2.2, are prone to contamination from wave action. We have examined a set of estimated TKE values from an ADCP deployed off the Welsh coast for a period covering roughly four spring–neap cycles, which is sufficiently long to capture all the most important modes of tidal variability. Since the site at which the ADCP was deployed was reasonably exposed to waves, and we had independent measurements of wave activity from a simultaneously-deployed buoy, this dataset offered a very good opportunity to investigate how well we can determine the true TKE from the estimate that the variance method actually yields.

It is immediately evident that the estimated TKE  $k_{ADCP}$  is indeed strongly influenced by waves (Fig. 2) and we can surmise that this kind of wave influence is typical of other non-sheltered energetic tidal sites. We started by showing that the first EOF mode captures a large majority of the variability in the  $k_{ADCP}$  record, consistent with the observation that estimated TKE is seemingly dominated by wave pseudo-TKE; subsequently, we were able to show that the mean vertical profile of  $k_{ADCP}$  is consistent with the presumption of significant wave activity.

A significant shortcoming of the EOF method for this purpose is that it cannot estimate the bias that wave action introduces to the

time-average of  $k_{ADCP}$ . We have worked around this by calculating a mean  $k_{ADCP}$  profile using only data from times of low wave action, and assuming that this mean profile is a good approximation to the portion of mean  $k_{ADCP}$  attributable to turbulence alone. The results in Fig. 6 show that this approach seems to be partially successful: the portion of the mean profile that we presume to be attributable to turbulence,  $\overline{k_t}$ , does not exhibit obviously wave-like behaviour except very near the surface.

To assess the effectiveness of the EOF analysis at separating waves and turbulence across the whole duration of the record, we considered the predicted values of near-surface pseudo-TKE due to wave action from both EOF analysis and linear wave theory. The comparison of these two estimates, as seen in Fig. 7, showed that the statistical and theoretical predictions of wave pseudo-TKE track one another very closely. A more detailed examination of the error, as illustrated by the results shown in Figs. 8 and 10–12, revealed a more complex picture. Although the absolute error is never very high, the relative error between the EOF estimate of wave pseudo-TKE and the linear theory estimate can spike very high; this motivated us to discuss possible criteria for times when it may not be suitable to use these methods to estimate wave pseudo-TKE. We suggest that estimates at times when  $EC_1 < 0$  i.e., when the first EOF mode is negative, may not be particularly meaningful. Excluding these times results in a sharp decline in the mean error between the two estimation methods.

The key test of the method presented in the paper is the decomposition shown in Fig. 9, and the improved version in Fig. 14. These results indicate that, where the wave contribution to this ADCP estimate of  $k$  significantly swamps the turbulent contribution for at least some times, empirical orthogonal function analysis can be used to find separate

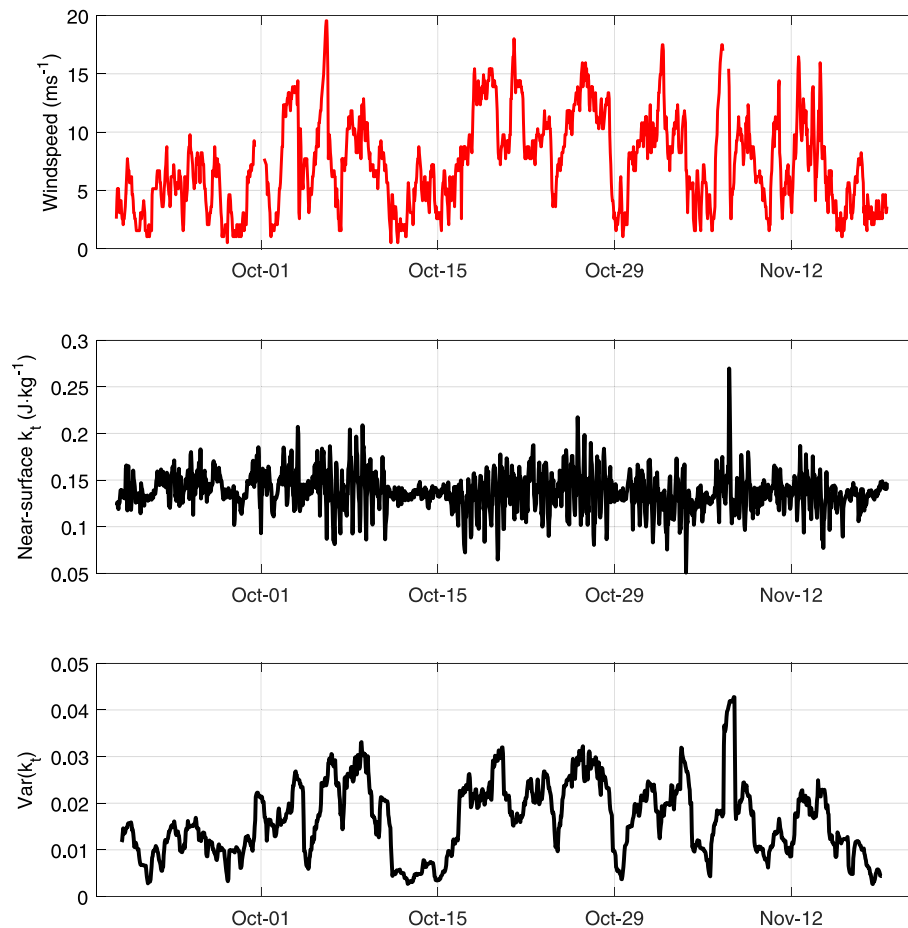


Fig. 15. Comparison of wind speed measured at RAF Valley weather station (top panel) with near-surface estimate of  $k_t$  from 2-mode EOF analysis (middle panel, cf. top panel of Fig. 14). Bottom panel shows rolling 20-sample variance of the near-surface  $k_t$  estimate.

wave and turbulent contributions to  $k_{ADCP}$  using a small number of data modes that contain most of the wave contribution. The method studied here permits a statistical (if not strictly physical) decoupling of the waves and turbulence where waves are sufficiently strong. At greater depths, and at sites where there is no strong wave activity, wave action does not contaminate along-beam velocity variances and reliable estimates of TKE can be obtained through standard analysis. Note that the method presented in this paper will work with ADCP data alone; the wave buoy data is used only to measure parameters informing the linear theory check on the EOF estimate of the wave contribution. This means the method can be applied even if there is no independent measurement of the wave properties, although this additional data is necessary to determine the optimum number of modes to include in the decomposition. In the absence of wave buoy data, it may be possible to use spectral analysis to estimate wave properties and thereby choose an optimum number of data modes, but this is not investigated here. Since the study presented in this paper does not directly filter measured ADCP velocities, there is also potential to achieve a better separation of waves and turbulence by combining spectral techniques applied to the velocity records with the statistical method described here applied to the derived bulk flow properties such as TKE.

#### CRediT authorship contribution statement

**M. Togneri:** Methodology, Software, Investigation, Validation, Writing – original draft, Funding acquisition. **I. Masters:** Supervision, Funding acquisition, Writing – review & editing. **I. Fairley:** Conceptualization, Methodology, Writing – review & editing.

#### Declaration of competing interest

The authors declare that they have no known competing financial interests or personal relationships that could have appeared to influence the work reported in this paper.

#### Acknowledgements

The authors acknowledge the support of the Welsh Assembly Government through the Sêr Cymru National Research network for Low Carbon, Energy and Environment, of EPSRC, United Kingdom through the projects SURFTEC (EP/P008628/1) and WTIMITS (funded via the Supergen ORE Hub, EP/S000747/1, through the Flexible Funding scheme), and of ERDF through the Interreg Atlantic Area project MONITOR (EAPA\_333/2016). The authors also acknowledged the support of the SEACAMS and SEACAMS 2 projects, part-funded by the European Regional Development Fund through the Welsh Government; the data analysed in this study were collected by researchers at Bangor University under these research programmes and are hosted on the IMARDIS data portal ([www.imardis.org](http://www.imardis.org)).

#### References

- Anis, A., Moum, J., 1995. Surface wave–turbulence interactions. Scaling  $\epsilon(z)$  near the sea surface. *J. Phys. Oceanogr.* 25 (9), 2025–2045.
- Appell, G.F., Bass, P., Metcalf, M.A., 1991. Acoustic Doppler current profiler performance in near surface and bottom boundaries. *IEEE J. Ocean. Eng.* 16 (4), 390–396.
- Björnsson, H., Venegas, S., 1997. A Manual for EOF and SVD Analyses of Climatic Data. CCGCR Report 97, pp. 112–134.

- Boufferrouk, A., Saulnier, J.B., Smith, G.H., Johanning, L., 2016. Field measurements of surface waves using a 5-beam ADCP. *Ocean Eng.* 112, 173–184.
- Clavero, M., Longo, S., Chiapponi, L., Losada, M., 2016. 3D flow measurements in regular breaking waves past a fixed submerged bar on an impermeable plane slope. *J. Fluid Mech.* 802, 490.
- Elasha, F., Mba, D., Togneri, M., Masters, I., Teixeira, J.A., 2017. A hybrid prognostic methodology for tidal turbine gearboxes. *Renew. Energy* 114, 1051–1061.
- Feddersen, F., Williams III, A., 2007. Direct estimation of the Reynolds stress vertical structure in the nearshore. *J. Atmos. Ocean. Technol.* 24 (1), 102–116.
- Guerra, M., Thomson, J., 2017. Turbulence measurements from five-beam acoustic Doppler current profilers. *J. Atmos. Ocean. Technol.* 34 (6), 1267–1284.
- Hay, A.E., Zedel, L., Craig, R., Paul, W., 2008. Multi-frequency, pulse-to-pulse coherent doppler sonar profiler. In: 2008 IEEE/OES 9th Working Conference on Current Measurement Technology. IEEE, pp. 25–29.
- IEC/TS 62600-201, 2014. Tidal Energy Resource Assessment and Characterisation. Standard. International Electrotechnical Commission.
- Jolliffe, I., 2011. *Principal Component Analysis*. Springer.
- Kirincich, A.R., Lentz, S.J., Gerbi, G.P., 2010. Calculating Reynolds stresses from ADCP measurements in the presence of surface gravity waves using the cospectra-fit method. *J. Atmos. Ocean. Technol.* 27 (5), 889–907.
- Kirincich, A.R., Rosman, J.H., 2011. A comparison of methods for estimating Reynolds stress from ADCP measurements in wavy environments. *J. Atmos. Ocean. Technol.* 28 (11), 1539–1553.
- Lewis, M., Neill, S., Robins, P., Ward, S., Piano, M., Hashemi, M., Goward-Brown, A., 2015. Observations of flow characteristics at potential tidal-stream energy sites. In: 11th European Wave and Tidal Energy Conference. Nantes.
- Lohrmann, A., Hackett, B., Røed, L.P., 1990. High resolution measurements of turbulence, velocity and stress using a pulse-to-pulse coherent sonar. *J. Atmos. Ocean. Technol.* 7 (1), 19–37.
- Lu, Y., Lueck, R.G., 1999a. Using a broadband ADCP in a tidal channel. Part I: Mean Flow and Shear. *J. Atmos. Ocean. Technol.* 16 (11), 1556–1567.
- Lu, Y., Lueck, R.G., 1999b. Using a broadband ADCP in a tidal channel. Part II: Turbulence. *J. Atmos. Ocean. Technol.* 16 (11), 1568–1579.
- McCann, G., 2007. Tidal current turbine fatigue loading sensitivity to waves and turbulence—a parametric study. In: Proceedings of the 7th European Wave and Tidal Energy Conference.
- McMillan, J.M., Hay, A.E., 2017. Spectral and structure function estimates of turbulence dissipation rates in a high-flow tidal channel using broadband ADCPs. *J. Atmos. Ocean. Technol.* 34 (1), 5–20.
- Milne, I., Day, A., Sharma, R., Flay, R., 2016. The characterisation of the hydrodynamic loads on tidal turbines due to turbulence. *Renew. Sustain. Energy Rev.* 56, 851–864.
- Milne, I., Sharma, R., Flay, R., 2017. The structure of turbulence in a rapid tidal flow. *Proc. R. Soc. A* 473 (2204), 20170295.
- Nezu, I., Nakagawa, H., 1993. *Turbulence in Open-Channel Flows*. Taylor & Francis.
- Nystrom, E.A., Rehmann, C.R., Oberg, K.A., 2007. Evaluation of mean velocity and turbulence measurements with ADCPs. *J. Hydraul. Eng.* 133 (12), 1310–1318.
- Piano, M., Ward, S., Robins, P., Neill, S., Lewis, M., Davies, A., Powell, B., Owen, A.W., Hashemi, R., 2015. Characterizing the tidal energy resource of the West Anglesey Demonstration Zone (UK), using Telemac-2D and field observations. In: Proceedings of the XXII TELEMAC-MASCARET Technical User Conference October 15–16, 2012. pp. 195–203.
- Preisendorfer, R., 1988. *Principal component analysis in meteorology and oceanography*. Elsevier Sci. Publ. 17, 425.
- Rosman, J.H., Hench, J.L., Koseff, J.R., Monismith, S.G., 2008. Extracting Reynolds stresses from acoustic Doppler current profiler measurements in wave-dominated environments. *J. Atmos. Ocean. Technol.* 25 (2), 286–306.
- Scherl, I., Strom, B., Shang, J.K., Williams, O., Polagye, B.L., Brunton, S.L., 2020. Robust principal component analysis for modal decomposition of corrupt fluid flows. *Phys. Rev. Fluids* 5 (5), 054401.
- Shaw, W.J., Trowbridge, J.H., 2001. The direct estimation of near-bottom turbulent fluxes in the presence of energetic wave motions. *J. Atmos. Ocean. Technol.* 18 (9), 1540–1557.
- Stacey, M.T., Monismith, S.G., Burau, J.R., 1999. Measurements of Reynolds stress profiles in unstratified tidal flow. *J. Geophys. Res.* 104 (C5), 10933–10949.
- Togneri, M., Jones, D., Neill, S., Lewis, M., Ward, S., Piano, M., Masters, I., 2017a. Comparison of 4-and 5-beam acoustic Doppler current profiler configurations for measurement of turbulent kinetic energy. *Energy Procedia* 125, 260–267.
- Togneri, M., Lewis, M., Neill, S., Masters, I., 2017b. Comparison of ADCP observations and 3D model simulations of turbulence at a tidal energy site. *Renew. Energy* 114, 273–282.
- Trowbridge, J., 1998. On a technique for measurement of turbulent shear stress in the presence of surface waves. *J. Atmos. Ocean. Technol.* 15 (1), 290–298.
- Veron, F., Melville, W.K., 1999. Pulse-to-pulse coherent doppler measurements of waves and turbulence. *J. Atmos. Ocean. Technol.* 16 (11), 1580–1597.
- Wolf, J., Prandle, D., 1999. Some observations of wave-current interaction. *Coast. Eng.* 37 (3–4), 471–485.